Magnetic Resonance Imaging 57 (2019) 156–164

Contents lists available at ScienceDirect

Magnetic Resonance Imaging

journal homepage: www.elsevier.com/locate/mri

Original contribution

Comparison of dynamic contrast-enhanced magnetic resonance imaging and contrast-enhanced ultrasound for evaluation of the effects of sorafenib in a rat model of hepatocellular carcinoma

Nina M. Muñoz[a], Adeeb A. Minhaj[a], Kiersten L. Maldonado[b], Charles V. Kingsley[b], Andrea C. Cortes[a], Houra Taghavi[b], Urszula Polak[a], Jennifer M. Mitchell[c], Joe E. Ensor[d], James A. Bankson[b], Asif Rashid[e], Rony Avritscher[a,*]

[a] Department of Interventional Radiology at The University of Texas M.D. Anderson Cancer Center, Houston, TX, United States of America
[b] Department of Imaging Physics at The University of Texas M.D. Anderson Cancer Center, Houston, TX, United States of America
[c] Department of Veterinary Medicine at The University of Texas M.D. Anderson Cancer Center, Houston, TX, United States of America
[d] The Houston Methodist Research Institute, Houston, TX, United States of America
[e] Department of Pathology at The University of Texas M.D. Anderson Cancer Center, Houston, TX, United States of America

ARTICLE INFO

Keywords:
Hepatocellular carcinoma
Sorafenib
Contrast-enhanced functional imaging
Vascular permeability
Tissue perfusion

ABSTRACT

Objectives: To compare the accuracy of contrast-enhanced ultrasound (CEUS) and Dynamic contrast-enhanced (DCE) magnetic resonance imaging (MRI) for the assessment of changes in tissue vascularization as result of sorafenib treatment in a rat model of hepatocellular carcinoma (HCC).

Methods: Male Buffalo rats with orthotopic liver tumors treated daily with 7.5 mg/kg sorafenib via oral gavage for 2 weeks (n = 9) were subject to DCE-MRI and CEUS 2 weeks after tumor implantation - right before treatment initiation - and also after treatment completion - right before tumor harvest. Untreated animals (n = 10) were used as control. Tumor tissue sections were stained for hematoxylin-eosin, pimonidazole, and CD34 for quantitative assessment of necrosis, hypoxia, and microvessel density (MVD), respectively.

Results: Of all the DCE-MRI parameters that were evaluated, only volume transfer constant (K^{trans}) measurements were significantly lower in sorafenib-treated tumors (0.18 vs 0.33 min^{-1}, $p < 0.01$), indicating a substantial decrease in vascular permeability caused by the therapy. This reduction was associated with decreased MVD (3.9 vs 10.8% CD34+ cells, $p < 0.01$), higher tumor necrosis (31.9 vs 21.8%, $p < 0.001$) and hypoxia (19.7 vs 10.5% pimonidazole binding, $p < 0.01$). Moreover, statistical analysis demonstrate significant correlation of DCE-MRI K^{trans} with histopathologic tissue necrosis ($r = -0.537$, $p < 0.05$) and MVD ($r = 0.599$, $p < 0.05$). Interestingly, none of the CEUS measurements were significantly different between the control and treatment groups, and did not show statistical correlation with any of the histopathological parameters assessed ($p > 0.05$).

Conclusions: Sorafenib-induced reduction in vascular permeability in this preclinical model of HCC is detected more accurately through DCE-MRI than CEUS, and DCE-MRI parameters strongly correlate with histopathological changes in tissue vascularization and tissue necrosis.

Abbreviations: AIF, Arterial Input Function; CEUS, contrast-enhanced ultrasound; CT, computed tomography; DCE, dynamic contrast-enhanced; FITC, Fluorescein Isothiocyanate; FLT, FMS-Like Tyrosine kinase; GFP, Green Fluorescent Protein; HRP, Horseradish Peroxidase; HCC, hepatocellular carcinoma; H&E, hematoxylin and eosin; $IAUC_{90}$, initial area under the curve at 90 s post-injection; ICC, Intrahepatic Cholangiocarcinoma; MRI, magnetic resonance imaging; MVD, microvessel density; PDGF, Platelet-Derived Growth Factor; PDGFR, Platelet-Derived Growth Factor Receptor; PE, peak enhancement; PET, positron emission tomography; Pimo, pimonidazole; mRECIST, Modified Response Evaluation Criteria in Solid Tumors; ROI, Regions-Of-Interest; TTP, time-to-peak; VEGF, Vascular Endothelial Growth Factor; VEGFR, Vascular Endothelial Growth Factor Receptor; WiR, wash-in rate

* Corresponding author at: Department of Interventional Radiology, Unit 1471, The University of Texas M.D. Anderson Cancer Center, PO Box 301402, Houston, TX 77230-1402, United States of America.
E-mail address: rony.avritscher@mdanderson.org (R. Avritscher).

https://doi.org/10.1016/j.mri.2018.11.012
Received 7 June 2018; Received in revised form 25 October 2018; Accepted 17 November 2018

1. Introduction

Hepatocellular carcinoma (HCC) ranks as the third leading cause of cancer death and as the sixth most common neoplasm [1]. Most patients are diagnosed at advanced stage [2,3] and do not qualify for curative therapies. The oral multikinase inhibitors sorafenib and regorafenib are currently the only agents proven to improve survival for patients with advanced-stage HCC [4–6] but their overall antitumor efficacy remains limited: the median overall survival for both systemic therapies is only 3 months longer than that of the placebo, and with only a subset of patients benefiting from treatment [4,7]. Reliable imaging biomarkers capable of consistently and accurately identifying the biological manifestations of tumor response would enable timely adjustments of treatment strategy, thus potentially improving outcomes and sparing unnecessary toxicity and cost of an ineffective therapy.

Oral multikinase inhibitors suppress both tumor growth - by targeting serine/threonine kinases of the Raf/MEK/ERK pathway, and angiogenesis - by targeting VEGFR1-3, PDGFR-β, and FLT3 tyrosine kinases, which block VEGF - and PDGF-dependent new blood vessel formation [8]. Because of the complexity of the effect of sorafenib on tumor biology, response to molecular-targeted therapies like this as well as to loco-regional interventional approaches is assessed according to mRECIST (Modified Response Evaluation Criteria in Solid Tumors) criteria, which are primarily based on contrast-enhanced radiologic imaging techniques.

Contrast-enhanced functional imaging studies are capable of reliably assessing tissue perfusion during therapy and have been used successfully to monitor response [9–11]. Functional imaging studies such as dynamic contrast-enhanced (DCE) magnetic resonance imaging (MRI) and computed tomography (CT), contrast-enhanced ultrasound (CEUS), positron emission tomography (PET) have all been successfully used to monitor response to antiangiogenic therapies [9–14]. Among these functional imaging tools, DCE-MRI has the longest track record in monitoring antivascular response having been successfully used in this role since the early 2000s [15–18]. This technique gained popularity due to its ability to non-invasively quantify multiple simultaneous parameters of vascular physiology, such as blood flow, vascular surface area and vascular permeability.

In the context of HCC assessment, several small clinical studies (< 45 patients enrolled) have shown the relevance of DCE-MRI parameters as potential predictors of treatment outcomes such as time-to-progression and overall survival. Zhu and colleagues, for instance, demonstrated that both K^{trans} and K_{ep} values are significantly reduced in advanced HCC cases after treatment with sunitinib monotherapy. Moreover, they showed that K^{trans} values were inversely correlated with disease progression, and that patients with partial response/stable disease had a two-fold or greater decrease in K^{trans} as compared to those with progressive disease [19]. Yopp and collaborators found that changes in iAUC90 and iAUC180 caused by treatment with floxuridine and dexamethasone in combination with bevacizumab in patients with primary liver cancer (i.e. HCC or ICC) were inversely correlated with time-to-progression. Interestingly, they did not find statistical correlation between K^{trans} and time-to-progression [20]. In another study, Zocco et al. reported that alterations in K^{trans} values resulting from treatment with sorafenib and metronomic tegafur/uracil to patients with advanced HCC correlated with tumor response, progression free- and overall survival [21]. The main limitation of DCE-MRI lies in the challenges of standardizing imaging biomarkers, because unlike serological markers, changes in technical parameters of image acquisition and processing can cause substantial variations between different studies or even within the same study at different time points.

In comparison to DCE-MRI, the use of functional parameters from CEUS for evaluation of treatment response in HCC has been more limited. Nonetheless, a few reports have described that reduction in tumor perfusion after transarterial chemoembolization or targeted therapies, is reflected in significant changes in parameters such as peak enhancement (PE), wash-in rate (WiR), and Area Under the time-intensity Curve (AUC) [22–25], and some of the studies have suggested that such alterations could be used as predictors of progression-free survival and even major adverse events [22,24,25]. Importantly, even though some of the limitations that affect DCE-MRI image acquisition and processing also apply to CEUS, this modality of ultrasound imaging offers substantial benefits such as availability, low cost, no radiation, and no nephrotoxicity, which make it an attractive alternative for monitoring angiogenesis inhibitor therapies with the considerable advantage of allowing multiple repeated longitudinal measurements [21].

Hence, the purpose of this study was to establish an effective sorafenib treatment protocol in a preclinical HCC model in which to assess whether functional contrast-enhanced imaging with ultrasound can provide comparable information to that of magnetic resonance by accurately depicting the effect of sorafenib therapy on tumor biology.

2. Materials and methods

2.1. Cell lines and reagents

A derivative of the rat hepatoma cell line McA-RH7777 (ATCC, Manassas VA) stably expressing the firefly luciferase and GFP reporter genes was used to generate an orthotopic syngeneic HCC model. To ensure consistency, the cells implanted in the animals were kept in culture for no > 4–5 passages prior to inoculation, and GFP expression was always > 90% as determined by flow cytometry analysis.

200 mg sorafenib tablets (Bayer, Whippany NJ) crushed into a fine powder and diluted in a 1:1 solution of Kolliphor EL (Sigma Aldrich, St. Louis MO) and 95% ethanol to a concentration of 12 mg/mL were used for oral gavage.

The hypoxia marker pimonidazole hydrochloride (Hypoxyprobe™-1), antibodies anti-pimonidazole FITC-conjugated (HP-FITC-MAb1), and anti-FITC HRP-conjugated were purchased from Hypoxyprobe (Burlington, MA). Anti-CD34 antibody (ab81289) was purchased from Abcam (Cambridge, MA).

2.2. Animal tumor model

Buffalo rats obtained from Charles River Laboratories (Wilmington, MA) were used to establish a breeding colony at our institution.

For tumor cell inoculation, 10^6 cells in 0.1 mL of saline solution with 2% normal rat serum (Sigma Aldrich, St. Louis MO) were injected in the subcapsular region of the left medial lobe of 19 male buffalo rats of 3–4 months of age. A piece of hemostatic gauze was applied on the site of injection, and a two-layer suture was then performed to close the abdomen.

Bioluminescence and T2-weighted MR imaging were performed weekly to assess tumor growth. The tumors were outlined by expert imaging technicians, and the volume of each tumor was estimated using the ellipsoid formula V = 0.52 × width × length × height, where the width and length were determined in the axial plane and the height in the coronal plane. Two weeks after tumor implantation, the animals were randomly assigned to remain untreated (n = 10) or to receive a daily dose of 7.5 mg/kg sorafenib by oral gavage (n = 9) for 2 additional weeks.

All tumors were harvested four weeks post-implantation, > 90 min after administering an intraperitoneal injection of 60 mg/kg pimonidazole, and immediately after CEUS and DCE-MRI were performed. Tissue specimens were fixed in 10% neutral buffered formalin and processed following standard procedures.

2.3. Imaging

2.3.1. Bioluminescence

10 min before bioluminescence imaging, an aqueous solution of D-Luciferin (1 mg/mL; Perkin Elmer, Waltham MA) was injected into the rats intravenously at 150 mg/kg. The rats were imaged individually using an IVIS Lumina XRMS bioluminescence imaging system (Perkin Elmer, Waltham MA). Photons emitted from the luciferase-expressing tumor cells were measured in standardized Regions-Of-Interest (ROIs) and quantified using the software program Living Imaging (Caliper Life Science, Waltham MA [26]. To standardize the regions of interest, we created an ROI that fully encompassed the entire liver. This ROI was saved into the analysis software and then loaded and applied to all subsequent animals.

2.3.2. Dynamic-enhanced magnetic resonance

Animals were anesthetized with 2% isoflurane and were placed in the prone position on the MRI sled. Imaging was carried out using a 4.7 T small animal MR scanner (Biospec, Bruker Biospin MRI, Inc., Billerica, MA) using a transmit/receive volume coil with a 72 mm inner diameter. Coronal and axial RARE T2-weighted images ((Cor) TR = 3000 ms, (Ax)TR = 1800 ms; TE = 40 ms; RARE factor = 8; averages = 3; matrix = 256 × 256; slice thickness = 1.50 mm; slice gap = 0.50 mm, FOV = 60 × 60 mm) were used for anatomic imaging to confirm animal position and tumor location. High-resolution axial T1-weighted fast spoiled gradient echo (FSPGR) images (TR = 140 ms; TE = 3.5 ms; average = 4; matrix = 256 × 256; spatial resolution = 0.234 mm/px; slice thickness = 1.50 mm; slice gap = 0.50 mm, excitation angle = 50°; FOV = 60 × 60 mm) were acquired before and after administration of contrast. DCE-MRI data was acquired using a FSPGR sequence (TR = 40 ms, TE = 1.6 ms; Average = 1; matrix = 128 × 96; slice thickness = 2.00 mm; slice gap = 0.50 mm; excitation angle = 35°; FOV = 80 × 60 mm; no. of repetitions = 90). 0.2 mmol/kg dose of gadopentetate dimeglumine (Magnevist, Bayer Healthcare Pharmaceuticals, Wayne NJ) was administered via tail vein catheter over a 10 s period beginning 1 min after the start of the DCE-MRI acquisition. We assumed a baseline T1 value of 1800 ms for tumor tissue based on a population of variable flip angle FSPGR measurements (data not shown).

The DCE-MRI analysis has been described elsewhere [27]. In summary, quantitative and semi quantitative parameters were calculated for each dataset using Matlab (MathWorks, Natick, MA). ROIs delineating the tumors were manually drawn in the mid-section plane, and pixels contributing to the Arterial Input Function (AIF) were manually selected in nearby vessels based on temporal enhancement characteristics and area-under-the-curve maps.

Pharmacokinetic (PK) analysis of dynamic data was carried out using the extended Tofts' model [28,29]. The normalized initial area under the curve was calculated by integrating signal enhancement to 90 s post-injection and normalizing to vascular enhancement. Non-enhancing tumor voxels with a very low NIAUC90 (< 5% of the tumor average) were excluded from the pharmacokinetic analysis.

2.3.3. Contrast-enhanced ultrasound

All animals were imaged with a high-frequency small-animal ultrasound system (Vevo® 2100, FUJIFILM, ON, Canada) utilizing a 21-MHz linear ultrasound array (LZ-250, FUJIFILM VisualSonics). The imaging focus and gain settings were kept constant across all imaging acquisitions. A matching brightness mode (B-mode) ultrasound frame was acquired for each contrast imaging frame. Tumor margins were manually segmented based on the B-mode data set for post-processing. The transducer array was adjusted to an imaging slice near the mid-section of the tumor that contained the largest tumor cross-section. Contrast imaging parameters were as follows for all acquisitions: power = 6%; beam width = 'Standard'; frame rate = 12 fps. Untargeted microbubble contrast (MicroMarker®, FUJIFILM) was re-suspended according to manufacturer's preparation protocol with 150 μL of the agent administered through a bolus tail-vein injection at an infusion rate of 6 μL/s. Imaging acquisition was initiated 2 s prior to the injection and continued for an additional 100 s. Output parameters, i.e., peak enhancement (PE), time to peak (TTP) and wash-in rate (WiR) were calculated using the VevoCQ®, FUJIFILM software package across the tumor mid-section plane. These commonly used parameters were selected to express both blood-volume based (peak enhancement), as well as flow-rate based (time to peak and wash-in rate) measurements. We chose to focus on these first-pass perfusion variables for better comparability with MRI values. Thus, we did not evaluate microbubble replenishment parameters, which reflect rate of contrast inflow after bursting microbubbles within the field of view.

2.4. Immunohistochemistry and automated image analysis

Serial sections were obtained from paraffin-embedded tissues and, to the extent possible, consecutive sections were stained with hematoxylin and eosin (H&E) or subject to immunohistochemistry staining for pimonidazole adducts or CD34 following the recommendations of the manufacturers of the antibodies.

All histology slides were digitized with an Aperio ScanScope AT2 slide scanner (Leica Biosystems Inc., IL). Under the supervision of an experienced and blinded pathologist, the Aperio ImageScope Software V12.0.1.5027 (Leica Biosystems Inc., IL) was used for the manual segmentation of all the tumor tissue present in the histology section corresponding to the mid-section plane of the tumor. The same software

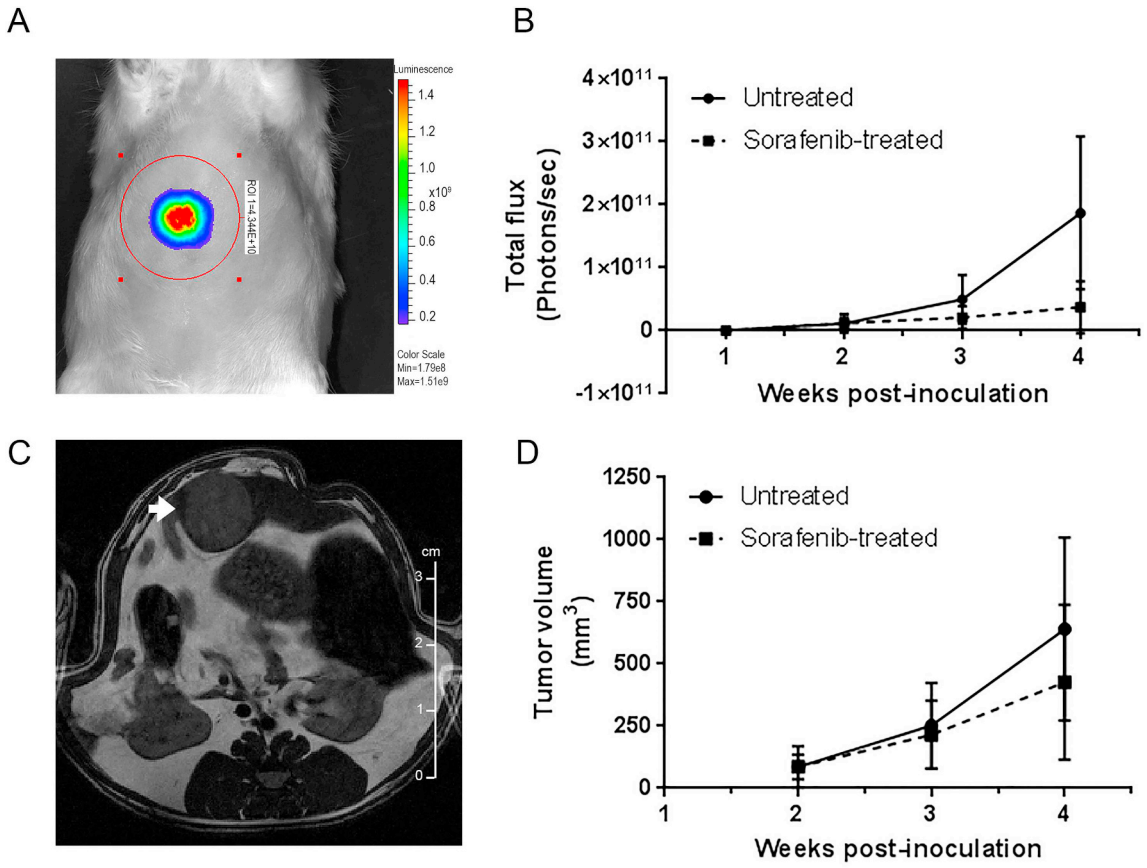

Fig. 1. HCC progression in the Buffalo rat orthotopic model. A. Detection of bioluminescent McA-RH7777 cells via IVIS 3 weeks post-inoculation. B. Weekly evaluation of luciferase enzymatic activity shows a slower rate of increase in the animals receiving treatment compared to the untreated controls. The graph represents mean signal at each time point and the error bars correspond to the 95% confidence intervals (CI) C.T2-weighted MR image of solitary liver tumor (white arrow) obtained in a Bruker 4.7 T magnet. D. Weekly tumor volume assessment in the untreated and sorafenib-treated rats demonstrates the effect of the treatment on tumor growth. The graph represents mean tumor volume at each time point and the error bars correspond to the 95% CI.

package was used for the quantification of tumor tissue necrosis (H&E), hypoxia (pimonidazole IHC), and microvessel density – MVD – (CD34 IHC) present in all the neoplastic tissue detected in the selected tissue sections.

2.5. Statistical analysis

Imaging parameter differences between the untreated and sorafenib-treated animals were investigated analytically by Wilcoxon rank-sum tests and graphically by box and whisker plots. Spearman's rank correlation coefficient was used to assess the presence of a pairwise monotonic relationship between imaging parameters. All analyses were conducted using SAS 9.4. Statistical significance was defined as $p < 0.05$.

3. Results

3.1. Sorafenib treatment prevents tumor growth in this HCC rat model

In vivo bioluminescence measurements demonstrated that, in most cases, luciferase activity in the untreated tumors increased exponentially over the 3-week period in which it was evaluated. In contrast, luciferase enzymatic activity decelerated, and in several instances plateaued, once the sorafenib treatment was initiated 2 weeks after tumor inoculation (Fig. 1A–B). Similarly, tumor volume measurements based on T2-weighted MR images demonstrated that while the tumor growth rates continued to increase in most of the untreated animals during the last week of follow-up, they remained constant for most animals in the sorafenib-treated cohort (Fig. 1C–D). These findings demonstrate that tumor growth rates in this animal model are

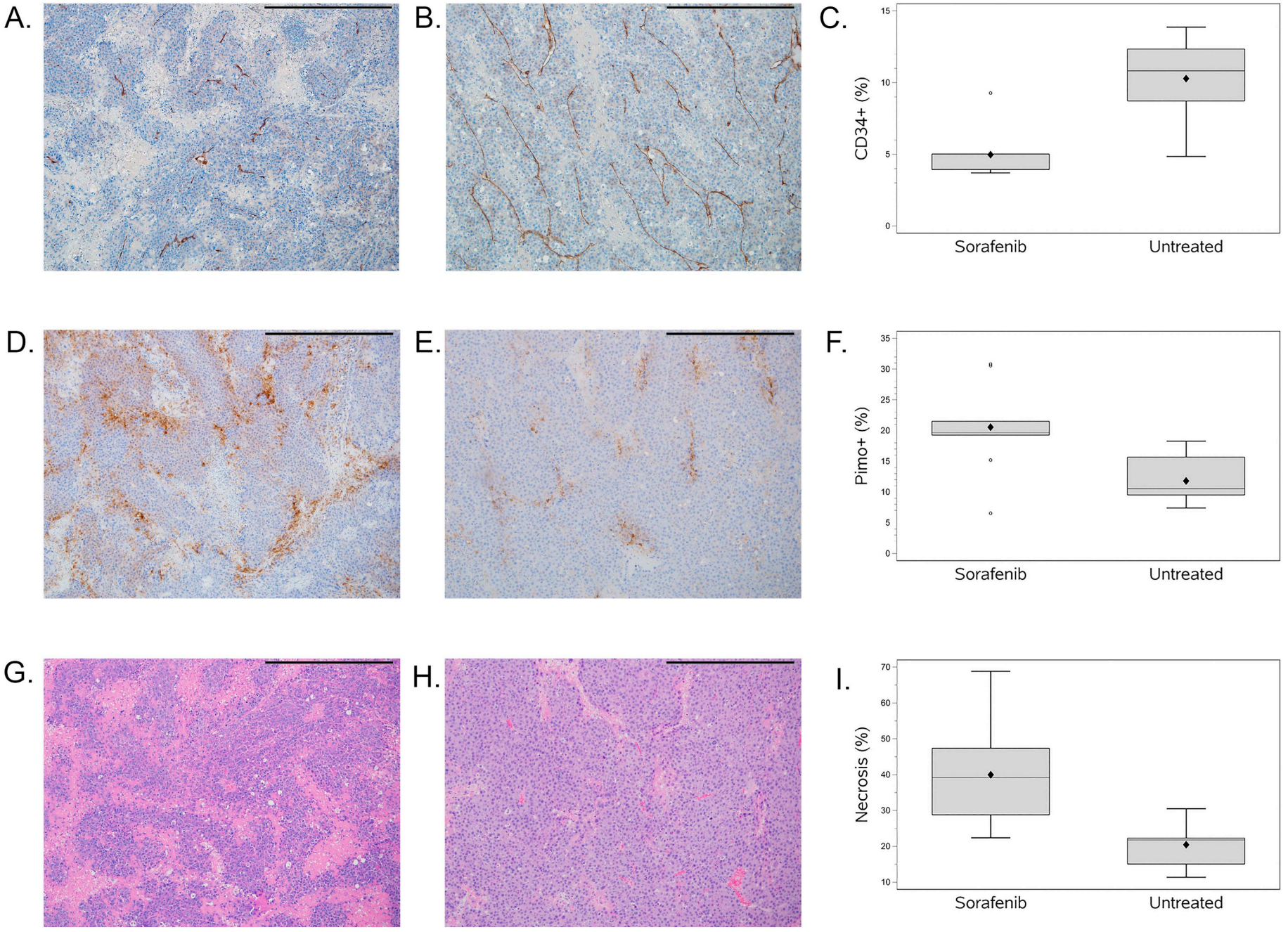

(continued on next page)

Fig. 2. Characteristic examples of sorafenib-treated (A, D, G) and untreated tumors (B, E, H). A–B, CD34 staining illustrates the decrease in tumor tissue microvessel density after multikinase inhibitor treatment. C. Box and whiskers plot of CD34 nuclei in both groups. D–E, Pimonidazole immunohistochemistry demonstrates the rise in tumor tissue hypoxia associated with this systemic treatment. F. Box and whiskers plot of pimonidazole positive cells in both groups. G–H, H&E stained tissue sections show the increase in tumor tissue necrosis after multikinase inhibitor treatment. I. Box and whiskers plot of necrotic areas in control and treatment groups. The scale bars in the micrographs represent 500 μM.

Table 1
Histopathological and immunohistochemical characteristics of the liver tumors.

Group		Necrosis (%)*	Pimonidazole + (%)*	CD34 + (%)*
Untreated	Median	21.78	10.54	10.82
	95% confidence interval	13.86–25.7	8.33–15.81	7.99–13.87
Sorafenib	Median	39.17	19.67	3.98
	95% confidence interval	25.28–47.38	15.53–30.90	3.70–9.41

All three parameters: necrosis, hypoxia (pimonidazole+), and microvessel density (CD34+) are significantly different between the two groups.

* $p < 0.05$ based on a Wilcoxon rank-sum test.

consistent, and the response to multikinase treatment recapitulates previous reports on rodent models of sorafenib treatment for HCC [30–33].

3.2. Sorafenib treatment inhibits tumor vascularization and promotes tumor tissue hypoxia and necrosis in this animal model

In order prevent any bias in the analyses and to account for the typical tumor tissue heterogeneity, an automated image analysis of all the tumor tissue present in the histology sections corresponding to the mid-section plane of the tumors was carried out. The analyses of tissue sections stained for the endothelial cell marker CD34 demonstrated that the sorafenib regimen effectively inhibited tumor tissue vascularization. The percentage of CD34 positive cells detected in the sorafenib-treated tumor tissues was 2.7 times less than in the untreated samples (Fig. 2A–C). Additionally, the reduction in the number of vessels in the treated tumors was associated with marked increases in the percentage of hypoxic and necrotic areas in the tumor tissue (Fig. 2D–I). Both hypoxia and necrosis were almost double in the sorafenib-treated samples as compared to the control tumors (1.8- and 1.9-fold increase, respectively - Table 1). Statistical analyses further confirmed a significant correlation between MVD and tumor tissue necrosis (Spearman correlation $r = -0.644$, $p < 0.05$) as well as between necrosis and hypoxia ($r = 0.556$, $p < 0.05$). Taken together, these results show that in spite of the relatively low dose and short treatment duration used here, the response to sorafenib therapy in this orthotopic HCC rat model was characterized by a potent antivascular effect that could definitely contribute to an overall hypoxic tumor microenvironment and to tumor cell death.

3.3. DCE-MRI shows higher sensitivity than CEUS for detection of sorafenib-induced vascular changes

Evaluation of tumor tissue vascularization through DCE-MRI showed that volume transfer constant (K^{trans}) values were significantly lower in the sorafenib-treated group compared with untreated animals (median 0.56 v 0.27, $p = 0.0047$– Table 2). K^{trans} measurements were also strongly correlated to histolopathological features of tumor tissue necrosis (Spearman correlation $r = -0.536$, $p < 0.05$) and MVD density (Spearman correlation $r = 0.599$, $p < 0.05$), respectively. Notably, no significant differences between control and treated tumors were found for other quantitative DCE-MRI and CEUS parameters, including blood plasma volume (ν_p), the reverse flux rate constant between the extravascular extracellular space and plasma (k_{ep}), and the normalized initial area under the curve at ($NIAUC_{90}$), PE, TTP, and WiR (Supplementary figure). This result supports the concept that DCE-MRI performs better than CEUS to accurately depict changes in vascular permeability, caused by systemic treatment with multikinase inhibitors (Fig. 3).

Table 2
Contrast-enhanced functional parameters of the liver tumors.

Group		K^{trans}*	k_{ep}	V_p	$IAUC_{90}$	PE	TTP	WiR
Untreated	Median	0.56	0.42	0.19	0.68	29.15	11.50	5.62
	95% confidence interval	0.40–1.06	0.36–0.55	0.09–0.30	0.48–0.94	11.20–49.30	5.80–22.81	1.98–21.20
Sorafenib	Median	0.27	0.50	0.16	0.54	20.70	9.96	6.13
	95% confidence interval	0.17–0.52	0.30–0.81	0.11–0.26	0.34–0.87	6.86–219.00	7.18–26.99	2.03–277.00

The only statistically significant difference between the 2 groups is in the median K^{trans}.
* p = 0.0043 based on a Wilcoxon rank-sum test.

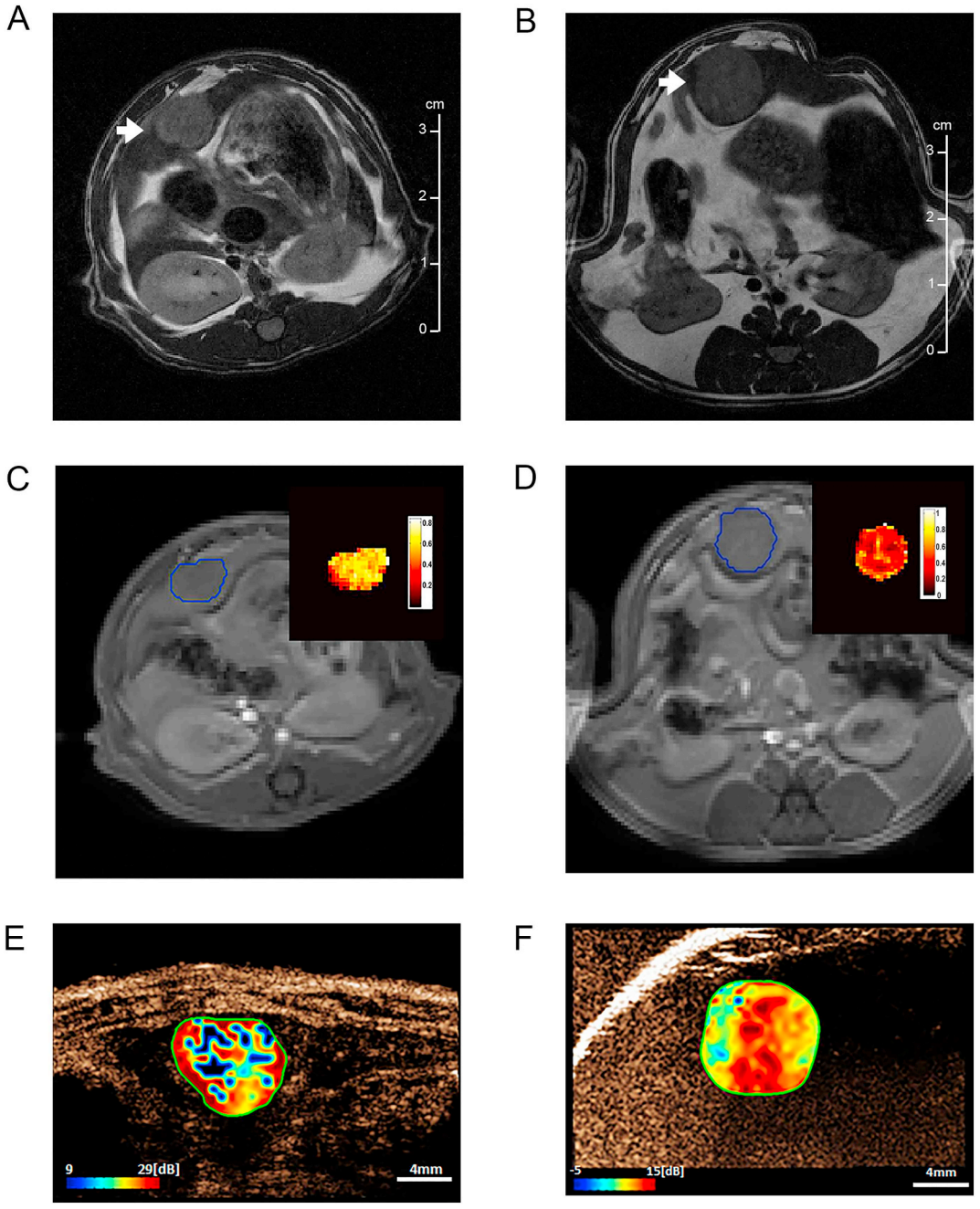

Fig. 3. Representative images of untreated (A, C, E) and sorafenib-treated tumors (B, D, F). A–B, T2-weighted MR scans of single liver neoplasms (indicated with white arrows). C–D, T1-weighted MR scans with insets showing DCE-MRI K^{trans} demonstrate a significant reduction in vascular permeability after sorafenib treatment. E–F, CEUS images with overlaid maps of peak enhancement highlighting the marked contrast in tumor perfusion between untreated and sorafenib tumors.

4. Discussion

Imaging biomarkers of treatment efficacy are essential for timely decision-making during multikinase inhibitor therapy in patients with advanced HCC. Because these therapeutic agents not only induce tumor cell death but also inhibit angiogenesis, traditional radiographic evaluation centered on tumor size underestimates response [34], and to help better characterize treatment-related vascularity changes, functional contrast-enhanced imaging studies are required [9–11]. Moreover, current treatment surveillance strategies can be improved by establishing the ability of different contrast-enhanced cross-sectional imaging modalities to accurately and consistently detect the biological effects of sorafenib treatment. The results of the present study demonstrate that in a preclinical HCC model, DCE-MRI is superior to CEUS in accurately depicting early alterations in vascular permeability caused by short-term therapy with sorafenib.

Sorafenib has a complex mechanism of action with multiple known targets and a plethora of biological effects. Preclinical and clinical studies have demonstrated that in HCC, sorafenib simultaneously targets both the underlying tumor vasculature, as well as tumor cell viability [35]. Specifically, the inhibitory activity on tyrosine kinase receptors including VEGFR 1-3 and PDGFR-α and -β has been shown to reduce endothelial cell proliferation and microvascular density in tumors [36]. This decrease of vasculature is associated with elevated tumor hypoxia, even after short-term treatment, as well as increased levels of cell death and tumor central necrosis [37]. Additionally, sorafenib causes tumor growth inhibition in a cell-autonomous fashion by inhibiting Raf/MEK/ERK signaling in the tumor cells [35].

Our rat HCC model reproduced the anti-tumor effects of sorafenib, even after short-term administration of relatively conservative doses of the drug: the standard human dose of sorafenib is 800 mg daily, which for a reference body weight of 60 kg, it would roughly correspond to 11 times the dose we used in our experimental rats (i.e. 7.5 mg/kg/day). Antiangiogenic and antitumor effects were reflected in reduction in tumor vascularity as assessed by immunohistochemical staining for CD34, increased tumor hypoxia by pimonidazole staining and increased tumor necrosis. These findings further establish the relevance of this model in the context of biomedical imaging research, in marked contrast to the study by Gross et al., which failed to establish a therapeutic effect of sorafenib treatment in a comparable rat HCC model [38]. Fundamental technical differences between their model and ours may explain the opposing findings. First, Gross and collaborators limited sorafenib treatment to only one week and then discontinued the drug, significantly limiting treatment response. Second, the tumor cells were injected into the portal vein rather than via subcapsular implantation. This approach creates a pattern resembling diffuse metastatic disease with confluent tumor nodules making it difficult to monitor response with cross-sectional imaging, when compared to a single dominant tumor nodule that more closely emulates human HCC [38].

Several different functional imaging techniques have been used to quantitatively or semi-quantitatively assess these complex cellular and vascular changes during multikinase inhibitor therapy. Among these techniques, DCE-MRI is the modality most extensively tested to monitor efficacy of anti-angiogenic therapies [15]. This clinical penetrance stems from its ability to non-invasively gain critical insights into these different mechanisms of action, such as variations in tissue perfusion and vascular permeability. Our results are consistent with previous studies, where DCE-MRI was able to detect variations in tumor microcirculation with a significant decrease in the volume transfer constant (K^{trans}) two weeks after initiation of antivascular therapy in HCC, which was correlated to increased tumor necrosis and reduction in microvascular density [19,39]. Other relevant DCE-MRI biomarkers, such as ν_p, k_{ep}, and $NIAUC_{90}$ did not show statistically significant correlation with early tumor response in our experiments. The lack of significant differences in tumor perfusion between the groups may be a consequence of vessel normalization during multikinase inhibitor therapy. By inhibiting VEGF pathways, multikinase inhibitor treatment partially restores normal angiogenesis signaling within the tumor microenvironment with tightening of cell-cell junctions and active recruitment of pericytes. These changes cause a maturation effect on the tumor vasculature that can lead to decreased vascular permeability and increased tumor perfusion. Our DCE-MRI and CEUS tumor perfusion parameters may be a reflection of this effect.

Although evident alterations in blood flow are apparent in CEUS and DCE-MRI images within treated nodules, high spatial variability of areas of tumor devascularization surrounded by areas of markedly increased perfusion can hamper accurate comparisons between the groups by diluting anti-angiogenesis effect in analyzed tumors. These features could further explain why lower values observed in perfusion variables for both DCE-MRI and DCE-US in the treated group failed to reach expected statistical significance.

Contrast-enhanced ultrasound could become a viable imaging modality to monitor anti-angiogenesis therapy due to its low cost and lack of ionizing radiation, which enables repeated examinations during the course of treatment. Clinical studies have indeed shown the value of CEUS in predicting tumor response to sorafenib therapy in HCC patients by demonstrating a decrease in time-intensity curve values for tumor perfusion [21,22,24,25]. Nevertheless, our CEUS data did not show statistically significant differences in most quantitative parameters, such as PE, TTP, WiR after sorafenib treatment. This finding is in agreement with other preclinical studies that evaluated CEUS performance early in the course of sorafenib administration to rabbits bearing VX2 tumors [40], and with a recent clinical study directly comparing DCE-MRI with CEUS for prostate cancer detection and prediction of aggressiveness [41]. Moreover, our CEUS quantitative data did not significantly correlate with histological biomarkers of tumor response either. Unlike low-molecular-weight contrast used for DCE-MRI, second generation ultrasound contrast agents consist of microbubbles with a mean diameter on the order of 0.5–10 μm. Therefore, the agent is confined strictly to the vascular bed and does not leak into the extravascular space. Since our results support the notion that vascular permeability and not blood flow is the predominant vascular effect of sorafenib treatment, CEUS seems to be limited in its ability to detect the specific changes in tumor vascularization associated with the type of multikinase inhibitor regimen used in this animal model.

We acknowledge some limitations of our study. First, our orthotopic model lacks the underlying cirrhosis that is typical of HCC. Although this feature may interfere with the response to antiangiogenic therapies, the advantage of creating a dominant single nodule that optimally lends itself to cross-sectional imaging made this animal model ideal to compare different functional imaging modalities. Second, our study compared DCE-MRI and CEUS, while other functional imaging modalities imaging are also commonly used to monitor treatment response to sorafenib in HCC patients, namely DCE-CT and PET, were not considered. Nonetheless, since DCE-CT and DCE-MRI rely on quantification of similar phenomena, our results should also apply to DCE-CT, after appropriate optimization of CT parameters. While PET imaging displays high sensitivity and versatility with agents available to quantify a variety of biological features, the cost remains a major barrier to wider utilization [13]. Thirdly, CEUS images in rodent models are inevitably affected by their rapid heartbeat, high respiratory rates, and challenging venous access, leading to motion artifact, as well as occasional low volume delivery of microbubble contrast through tail vein access resulting in reduced signal-to-noise ratio. Motion compensation software was used here to minimize the influence of motion artifact in the final quantitative analysis. Lastly, it is important to note that is it possible that a higher dose and/or a longer sorafenib regimen could have resulted in better performance of CEUS because in spite of administering a lower relative sorafenib dose to our animals (the human full dose of 400 mg of sorafenib bid) for a short period of time, we did find a 29% reduction in PE in our experiments (Table 2).

5. Conclusions

Using a preclinical model that recapitulates histopathological features of sorafenib treatment in hepatocellular carcinoma, namely decreased microvascular density, increased tissue necrosis and hypoxia, we show that vascular permeability and not blood flow is the predominant vascular feature that is altered by this type of multikinase inhibitor regimen. Comparing CEUS and DCE-MRI, vascular permeability was the only change detected by imaging using the DCE-MRI vascular permeability parameter (K^{trans}).

Supplementary data to this article can be found online at https://doi.org/10.1016/j.mri.2018.11.012.

Declarations of interest

None.

Acknowledgements

This research was funded through the generous support of the John S. Dunn Foundation via the Distinguished Chair in Diagnostic Imaging; the CPRIT Individual Investigator Award RP160229 (R.A.), and the NIH/NCI through M. D. Anderson's Cancer Center Support Grant CA016672 used by the Small Animal Imaging and the Flow Cytometry & Cellular Imaging Core Facilities.

References

[1] Siegel RL, Miller KD, Jemal A. Cancer statistics, 2018. CA Cancer J Clin 2018;68(1):7–30.
[2] Lee JH, et al. Barcelona Clinic Liver Cancer staging system and survival of untreated hepatocellular carcinoma in a hepatitis B virus endemic area. J Gastroenterol Hepatol 2015;30(4):696–705.
[3] Giannini EG, et al. Prognosis of untreated hepatocellular carcinoma. Hepatology 2015;61(1):184–90.
[4] Llovet JM, et al. Sorafenib in advanced hepatocellular carcinoma. N Engl J Med 2008;359(4):378–90.
[5] Cheng AL, et al. Efficacy and safety of sorafenib in patients in the Asia-Pacific region with advanced hepatocellular carcinoma: a phase III randomised, double-blind, placebo-controlled trial. Lancet Oncol 2009;10(1):25–34.
[6] Bruix J, et al. Regorafenib for patients with hepatocellular carcinoma who progressed on sorafenib treatment (RESORCE): a randomised, double-blind, placebo-controlled, phase 3 trial. Lancet 2017;389(10064):56–66.
[7] Schott E, Ebert MP, Trojan J. Treatment of hepatocellular carcinoma with sorafenib - focus on special populations and adverse event management. Z Gastroenterol 2012;50(9):1018–27.
[8] Huynh H. Molecularly targeted therapy in hepatocellular carcinoma. Biochem Pharmacol 2010;80(5):550–60.
[9] Cyran CC, et al. In vivo monitoring of sorafenib therapy effects on experimental prostate carcinomas using dynamic contrast-enhanced MRI and macromolecular contrast media. Cancer Imaging 2013;13(4):557–66.
[10] Cyran CC, et al. Dynamic contrast-enhanced computed tomography imaging biomarkers correlated with immunohistochemistry for monitoring the effects of sorafenib on experimental prostate carcinomas. Invest Radiol 2012;47(1):49–57.
[11] Hahn OM, et al. Dynamic contrast-enhanced magnetic resonance imaging pharmacodynamic biomarker study of sorafenib in metastatic renal carcinoma. J Clin Oncol 2008;26(28):4572–8.
[12] Anderson H, et al. Measuring changes in human tumour vasculature in response to therapy using functional imaging techniques. Br J Cancer 2001;85(8):1085–93.
[13] Willmann JK, et al. Molecular imaging in drug development. Nat Rev Drug Discov 2008;7(7):591–607.
[14] Dobrucki LW, et al. Approaches to multimodality imaging of angiogenesis. J Nucl Med 2010;51(Suppl. 1):66S–79S.
[15] O'Connor JP, et al. Dynamic contrast-enhanced MRI in clinical trials of antivascular therapies. Nat Rev Clin Oncol 2012;9(3):167–77.
[16] Jayson GC, et al. Molecular imaging and biological evaluation of HuMV833 anti-VEGF antibody: implications for trial design of antiangiogenic antibodies. J Natl Cancer Inst 2002;94(19):1484–93.
[17] Galbraith SM, et al. Effects of 5,6-dimethylxanthenone-4-acetic acid on human tumor microcirculation assessed by dynamic contrast-enhanced magnetic resonance imaging. J Clin Oncol 2002;20(18):3826–40.
[18] Dowlati A, et al. A phase I pharmacokinetic and translational study of the novel vascular targeting agent combretastatin a-4 phosphate on a single-dose intravenous schedule in patients with advanced cancer. Cancer Res 2002;62(12):3408–16.
[19] Zhu AX, et al. Efficacy, safety, and potential biomarkers of sunitinib monotherapy in advanced hepatocellular carcinoma: a phase II study. J Clin Oncol 2009;27(18):3027–35.
[20] Yopp AC, et al. Antiangiogenic therapy for primary liver cancer: correlation of changes in dynamic contrast-enhanced magnetic resonance imaging with tissue hypoxia markers and clinical response. Ann Surg Oncol 2011;18(8):2192–9.
[21] Zocco MA, et al. Early prediction of response to sorafenib in patients with advanced hepatocellular carcinoma: the role of dynamic contrast enhanced ultrasound. J Hepatol 2013;59(5):1014–21.
[22] Lassau N, et al. Advanced hepatocellular carcinoma: early evaluation of response to bevacizumab therapy at dynamic contrast-enhanced US with quantification—preliminary results. Radiology 2011;258(1):291–300.
[23] Wiggermann P, et al. Degradable starch microspheres transarterial chemoembolisation (DSM-TACE) of HCC: Dynamic Contrast-Enhanced Ultrasonography (DCE-US) based evaluation of therapeutic efficacy using a novel perfusion software. Clin Hemorheol Microcirc 2012;52(2–4):123–9.
[24] Sugimoto K, et al. Hepatocellular carcinoma treated with sorafenib: early detection of treatment response and major adverse events by contrast-enhanced US. Liver Int 2013;33(4):605–15.
[25] Frampas E, et al. Advanced hepatocellular carcinoma: early evaluation of response to targeted therapy and prognostic value of Perfusion CT and Dynamic Contrast Enhanced-Ultrasound. Preliminary results. Eur J Radiol 2013;82(5):e205–11.
[26] Zhou M, et al. Single agent nanoparticle for radiotherapy and radio-photothermal therapy in anaplastic thyroid cancer. Biomaterials 2015;57:41–9.
[27] Ramirez MS, et al. Feasibility of multiple-mouse dynamic contrast-enhanced MRI. Magn Reson Med 2007;58(3):610–5.
[28] Tofts PS. Modeling tracer kinetics in dynamic Gd-DTPA MR imaging. J Magn Reson Imaging 1997;7(1):91–101.
[29] Tofts PS, et al. Estimating kinetic parameters from dynamic contrast-enhanced T(1)-weighted MRI of a diffusable tracer: standardized quantities and symbols. J Magn Reson Imaging 1999;10(3):223–32.
[30] Gu FM, et al. Sorafenib inhibits growth and metastasis of hepatocellular carcinoma by blocking STAT3. World J Gastroenterol 2011;17(34):3922–32.
[31] Runge A, et al. An inducible hepatocellular carcinoma model for preclinical evaluation of antiangiogenic therapy in adult mice. Cancer Res 2014;74(15):4157–69.
[32] Sieghart W, et al. Erlotinib and sorafenib in an orthotopic rat model of hepatocellular carcinoma. J Hepatol 2012;57(3):592–9.
[33] Roth GS, et al. Efficacy of AKT inhibitor ARQ 092 compared with sorafenib in a cirrhotic rat model with hepatocellular carcinoma. Mol Cancer Ther 2017;16(10):2157–65. https://doi.org/10.1158/1535-7163.
[34] Desar IM, et al. Beyond RECIST: molecular and functional imaging techniques for evaluation of response to targeted therapy. Cancer Treat Rev 2009;35(4):309–21.
[35] Liu L, et al. Sorafenib blocks the RAF/MEK/ERK pathway, inhibits tumor angiogenesis, and induces tumor cell apoptosis in hepatocellular carcinoma model PLC/PRF/5. Cancer Res 2006;66(24):11851–8.
[36] Jain RK. Molecular regulation of vessel maturation. Nat Med 2003;9(6):685–93.
[37] Chang YS, et al. Sorafenib (BAY 43-9006) inhibits tumor growth and vascularization and induces tumor apoptosis and hypoxia in RCC xenograft models. Cancer Chemother Pharmacol 2007;59(5):561–74.
[38] Gross C, et al. Model matters: differences in orthotopic rat hepatocellular carcinoma physiology determine therapy response to sorafenib. Clin Cancer Res 2015;21(19):4440–50.
[39] Murphy P, et al. Vascular response of hepatocellular carcinoma to pazopanib measured by dynamic contrast-enhanced MRI: pharmacokinetic and clinical activity correlations. Proc Intl Soc Mag Reson Med 2010;18. (Stockholm, Sweden).
[40] Kong WT, et al. Early treatment response to sorafenib for rabbit VX2 orthotic liver tumors: evaluation by quantitative contrast-enhanced ultrasound. Tumour Biol 2015;36(4):2593–9.
[41] Baur ADJ, et al. A direct comparison of contrast-enhanced ultrasound and dynamic contrast-enhanced magnetic resonance imaging for prostate cancer detection and prediction of aggressiveness. Eur Radiol 2018;28(5):1949–60.